Chapter 2

Synthesis and Activity of a New Catalyst for Hydroprocessing:

Tungsten Phosphide

2.1. Introduction

There has been considerable recent interest in the development of new
hydroprocessing catalysts because more efficient conversion of heavier oil fractions is
becoming increasingly important as world petroleum reserves are consumed and lower
quality base stocks are utilized. Hydrodenitrogenation (HDN) is the most desired
reaction in first-stage hydrocracking of heavy oil fractions such as vacuum gas oils (1),
preparing the liquid for cracking over acid catalysts which are poisoned by nitrogen
bases. Typical hydroprocessing catalysts are alumina supported bimetallic sulfides of
molybdenum or tungsten with either nickel or cobalt 'promoter' (2, 3, 4), and often
contain phosphorus as a secondary promoter (5, 6, 7, 8, 9, 10).

Recent developments in hydroprocessing catalysis include the introduction of novel
carbide and nitride compositions (11, 12, 13), the use of sulfides of early transition metals
(14, 15, 16, 17), the use of noble metals (18, 19, 20), and the use of zeolites (21, 22).

This chapter describes the synthesis and characterization of a new catalytic material,
tungsten phosphide, which has high activity for hydroprocessing. The catalyst is a
member of a class of compounds known as the transition metal phosphides, with metallic
or semiconducting properties and physical characteristics typical of intermetallic
compounds. There are only a few reports of the use of transition metal phosphides as

heterogeneous catalysts. Ni_2P and other phosphides have been applied as olefin hydrogenation catalysts (23, 24, 25, 26), and bulk Ni_2P and Co_2P were found to be active for denitrogenation of quinoline (27). Amorphous nickel phosphide prepared by chemical reduction has been reported to be active for hydrogenation of nitrobenzene to aniline (28). Recently, molybdenum phosphide was reported to be an active and stable HDN catalyst as well (29,30).

Bulk tungsten compounds which have been previously reported as hydroprocessing catalysts include the sulfide WS_2 (3, 4), the carbide WC (13), and the nitride W_2N (31, 32). Pure WS_2 samples with high specific surface area are typically prepared by decomposition of ammonium tetrathiotungstate (33, 34, 35, 36). High surface area tungsten carbide and nitride samples are obtained by temperature programmed reactions of WO_3 with methane and ammonia, respectively. The tungsten phosphide, WP, used in this study was prepared by the direct hydrogen reduction of a stoichiometric phosphate glass at moderate temperature.

Phosphorus is commonly used a secondary promoter in commercial hydroprocessing catalyst formulations (5, 8, 9, 10). In these catalysts phosphorus is introduced onto the alumina support by aqueous impregnation and is in the form of an oxide or phosphate on the surface. This is the first report of the synthesis and characterization of a tungsten phosphide catalyst, where the phosphorus is found in the reduced form in the bulk.

2.2.   Experimental

The starting material for the synthesis of tungsten phosphide was a tungsten phosphate. The phosphate was prepared by combining stoichiometric quantities of ammonium metatungstate, $(NH_4)_6W_{12}O_{39} \cdot xH_2O$ (Aldrich), and ammonium phosphate, $(NH_4)_2HPO_4$ (Aldrich, 99%), in sufficient distilled water to form a clear solution. Then the solution was evaporated to dryness and calcined in air at 773 K for 6 hours. The product, tungsten phosphate, was ground to a powder with a mortar and pestle for further use.

Tungsten phosphide, WP, was prepared from the tungsten phosphate precursor by means of temperature programmed reduction (TPR) with linear temperature ramps in flowing hydrogen. In the TPR procedure, 0.300 g of material were loaded in a quartz glass u-tube reactor and the effluent was monitored by a mass spectrometer (Ametek/Dycor MA100). In catalyst preparation, larger batches using up to 1.50 g of tungsten phosphate were prepared and combined to form the working WP catalyst. For the WP catalyst, the temperature was increased to 938 K at 0.0167 K s^{-1}, where it was held for 2 h before quenching in helium flow (67 μmol s^{-1}). The flow rate of hydrogen was maintained at 650 μmol s^{-1} g^{-1} starting material (300 cm^3(NTP) min^{-1} for 0.300 g metal phosphate) in all experiments.

Tungsten sulfide, WS$_2$, was prepared by decomposition of ammonium tetrathiotungstate, $(NH_4)_2WS_4$ (Aldrich, 99.9+%), in a 10% H$_2$S/H$_2$ mixture. The sample was prepared from three batches of 1.3 g of ammonium tetrathiotungstate heated at 0.0833 K s^{-1} in 870 μmol s^{-1} of 10% H$_2$S/H$_2$ to a final temperature of 678 K which was

held for 2 h. The syntheses of the high surface area WC and W_2N have been described in the literature (12, 13, 31, 32).

Reaction products were passivated progressively with 0.1% O_2/He (80 μmol s^{-1} for 12 h), 0.5% O_2/He (13 μmol s^{-1} for 2 h), then diffusive air exposure in the reactor tube for 24 h, before collection and storage. All gases were supplied by Air Products. The listed purity of hydrogen, helium, and carbon monoxide was 99.999 %, and that for oxygen was 99.99 %. These gases were passed through a water trap (Alltech) before contacting the samples. Specialty mixtures, including 0.5 % O_2/He, 30 % N_2/He, and 10 % H_2S/H_2 were used as received.

Chemisorption (CO uptake, O_2 uptake) and single point BET (Brunauer, Emmett, and Teller) nitrogen physisorption measurements were performed on samples directly after preparation, immediately after cooling to room temperature in helium, and these will be referred to here as *in situ* measurements. Characterizations performed on passivated, air-exposed samples rereduced in hydrogen for 2 h at 623 K, were used as the basis for hydroprocessing tests and are referred to in this report as *ex situ* measurements. Pulses of CO or O_2 (5.6 μmol) were passed over the sample to measure the total, dynamic gas uptake. Single-point BET surface area measurements were carried out by passing a 30% N_2/He gas mixture to the sample at liquid nitrogen temperature, then measuring the nitrogen desorbed as the sample was heated rapidly to room temperature.

X-ray diffraction (XRD) spectra were collected using a Scintag XDS-2000 X-ray diffractometer using Ni-filtered Cu K$_\alpha$ ($\lambda = 0.1541$ nm) radiation and a scan rate of $0.035^{o}\, 2\theta$ s^{-1}. Crystallite sizes were estimated from the XRD peak line-widths using the

method of Scherrer (37). The activation energy was calculated for the reduction reaction by the heating rate variation method of Redhead (38).

X-ray photoelectron spectroscopy (XPS) experiments were performed with a Perkin-Elmer 5000 surface analyzer. Samples were mounted on double-sided adhesive tape, and binding energies were referenced to adventitious carbon at 285.0 eV. Quantification was achieved using sensitivity factors published by the instrument manufacturer (39).

Hydrotreating was carried out at 3.1 MPa (450 psig), and 643 K (370 $^\circ$C), with 100 μmol s^{-1} (150 cm^3(NTP) min^{-1}) hydrogen flow, in a three phase up-flow fixed bed reactor operated as described previously (4). The feed liquid was prepared by combining tetralin (Aldrich, 99%), tetradecane (Fisher, 99%), quinoline (Aldrich, 99%), dibenzothiophene (Aldrich, 99%), and benzofuran (Aldrich, 99%) to create a liquid with composition summarized in Table 2.1. The so formed liquid was delivered to the catalyst at 8.33 x 10^{-5} dm^3 s^{-1} (5 cm^3 min^{-1}). Liquid product compositions were determined with a Hewlett Packard 5890A gas chromatograph, using a 50 m dimethylsiloxane column with 0.3 μm i.d. and 0.2 μm film thickness (Chrompack, CPSil 5B), on samples collected at 2-3 h intervals.

Table 2.1: Composition of liquid feed used for hydroprocessing reaction.

Component	mol%	wt%	N, S, O wppm	Delivery Rate μmol h^{-1}
quinoline	2.6	1.9	2000	580
dibenzothiophene	1.7	1.7	3000	380
benzofuran	0.6	0.4	500	130
tetralin	27	20	0	6100
tetradecane	68	76	0	15500

For the hydroprocessing reaction, the passivated WP catalyst was pretreated for 2 h at
623 K in 100 μmol s^{-1} (150 sccm NTP) of H$_2$, at a pressure slightly above 1 atm. The
WS$_2$ catalyst was pretreated at 578 K for 2 h under 100 μmol s^{-1} of 10 % H$_2$S/H$_2$. After
pretreatment, the reactor temperature and pressure were set to reaction conditions, and the
liquid flow was started.   Steady state was verified to be obtained in the last 30 h of a 60+
h reaction run. In this report, % HDN is defined as the total conversion of quinoline
minus the sum of nitrogen containing products, % HYD is the sum of N containing
quinoline intermediates, and % HDS is defined as the conversion of dibenzothiophene (as
no S containing intermediates were identified).

2.3.   Results

2.3.1. Synthesis of Tungsten Phosphide

A typical reduction profile of the reaction forming tungsten phosphide is presented in
Figure 2.1, along with *in situ* characterization results from intermediate samples. A small
amount of water of hydration is evolved near 373 K, otherwise, there is only a single
reaction peak produced by the reduction process.   The *in situ* surface areas and CO
chemisorption values shown in Figure 2.1 increase with temperature up to 893 K, then
begin to decrease.   The trends in these properties follow the water evolution profile.

X-ray diffraction spectra of quenched, passivated intermediates are shown in Figure 2.2. The starting material is amorphous and unchanged at 773 K. The single product of the reaction, WP, grows in smoothly as the reaction progresses.
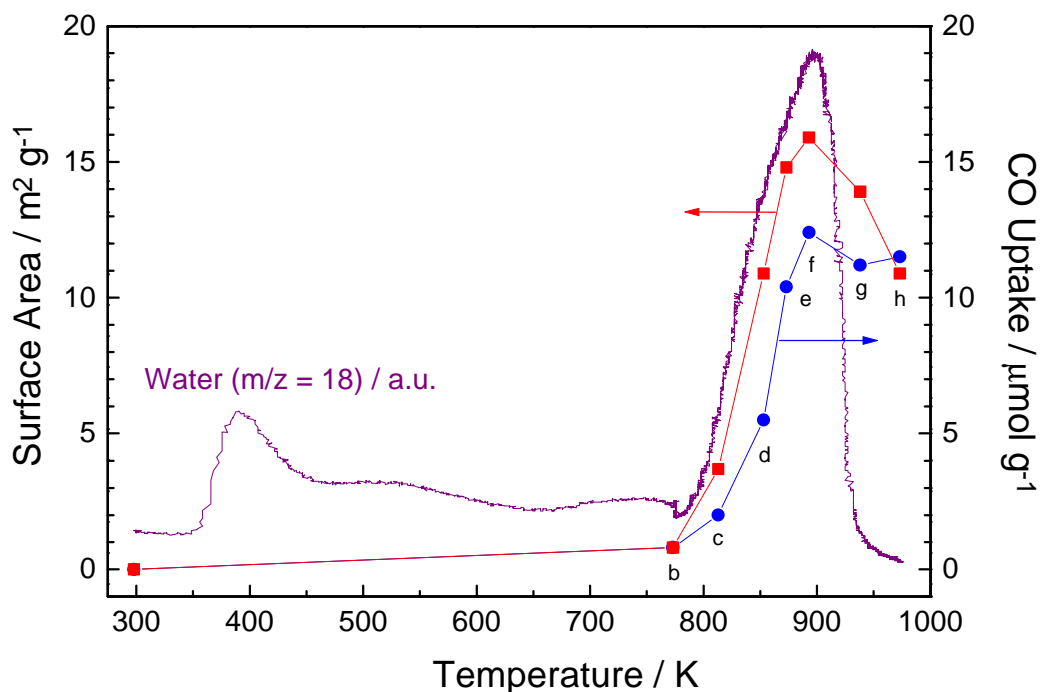

Figure 2.1: Water evolved during the synthesis of tungsten phosphide from tungsten phosphate glass. Samples were preheated to 773 K at 0.0833 K s^{-1}, then ramped at 0.0167 K s^{-1} to their final temperature. *In situ* surface area ( ) and CO uptake values ( ) of quenched intermediates are compared to the reaction progress. The letters b – h also correspond to XRD spectra of quench intermediate samples noted in Figure 2.2.
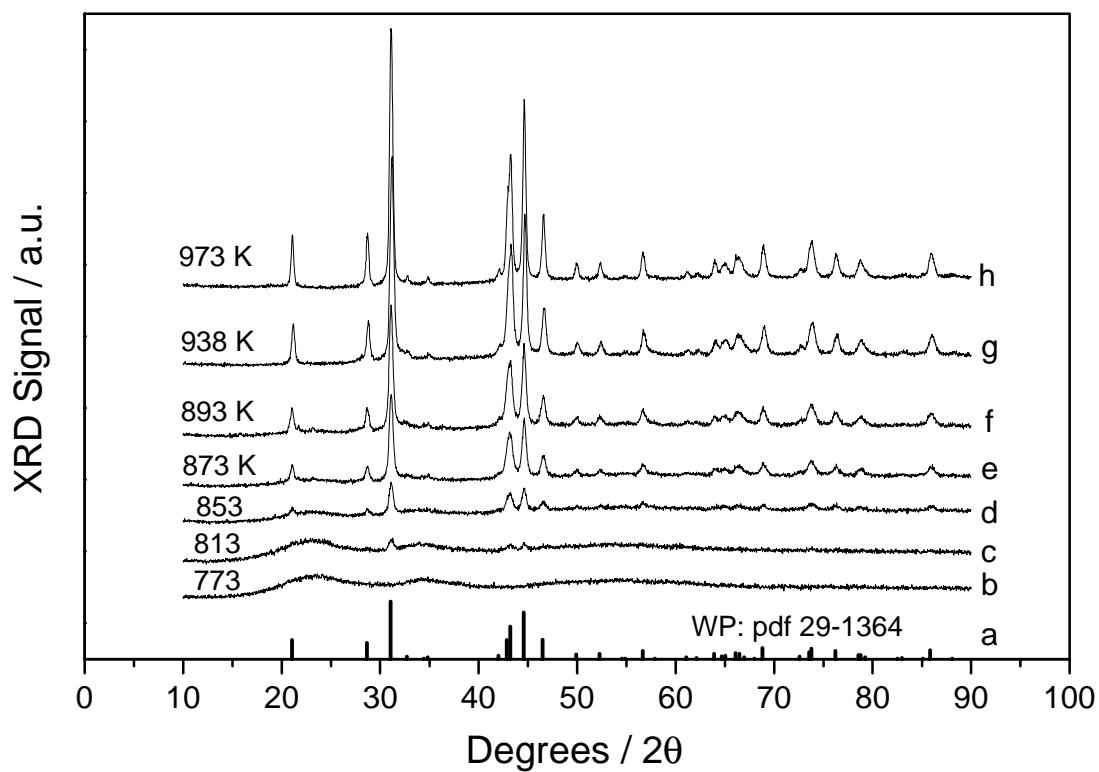
Figure 2.2: X-ray diffraction patterns of intermediate samples quenched at various temperatures after reduction in hydrogen at 0.0167 K s^{-1}. The letters b – h also correspond to BET surface area and CO chemisorption values of intermediate samples noted in Figure 2.1.

Tungsten phosphide adopts the orthorhombic manganese phosphide (MnP) structure type (strukturbericht designation B31: Space Group P_{bnm}), a structure which is closely related to the hexagonal NiAs structure type (40, 41), but in which lattice distortions accompany the formation of chains of phosphorus atoms (42).   The lattice parameters for WP are a_o = 0.6219 nm, b_o=0.5717 nm, and c_o = 0.3238 nm (43). An estimation of the surface site density is made based on the lowest index planes as follows. We find 2 atoms per cell in the (100) plane, leading to 0.0926 nm^2 per W atom, 2 atoms per cell in the (010) plane, giving 0.1007 nm^2 per atom in this plane, and 3 atoms per cell in the (001) plane, yielding 0.1185 nm^2 per W. The average is then calculated to be 0.1037 nm^2 per W, which is similar to the value of 0.103 nm^2 (10.3 Å^2) per Mo reported by Stinner et al. (30) for MoP.

Variation of the heating rate in WP synthesis from 0.00833 to 0.0833 K s^{-1} (i.e. over an order of magnitude) shifted the temperature maximum as noted in Table 2.2. From this data, a first order activation energy of 148 kJ mol^{-1} is calculated for the reduction process.

Table 2.2: Variation in the temperature corresponding to the maximum rate in the formation of WP as a function of heating rate.

Heating Rate K min^{-1}	Temperature Maximum K
0.5	862
1	893
2	934
3	952
5	1013

2.3.2. Catalyst Characterization

The WP catalyst was characterized before and after the hydroprocessing reaction by *ex situ* (defined above) BET surface area determination, *ex situ* CO chemisorption, and X-ray diffraction of air exposed samples. The surface area and CO chemisorption characteristics of the catalyst are reported in Table 2.3, and the XRD spectra are shown in Figure 2.3. These characteristics were effectively unchanged by catalytic reaction, and the results demonstrate that the WP bulk and surface are stable under reaction conditions. That the bulk WP phase is not altered by reaction is also verified by the stability of the lattice parameters and crystallite size (in the {011} directions) as reported in Table 2.4. The fresh tungsten sulfide catalyst had *ex situ* BET surface area of 37 m^2 g^{-1} and O_2 uptake of 58 μmol O g^{-1}.

Table 2.3: Comparison of *ex situ* measurements of BET surface area, CO chemisorption, and site density characteristics of WP catalyst, before and after hydrotreating study.

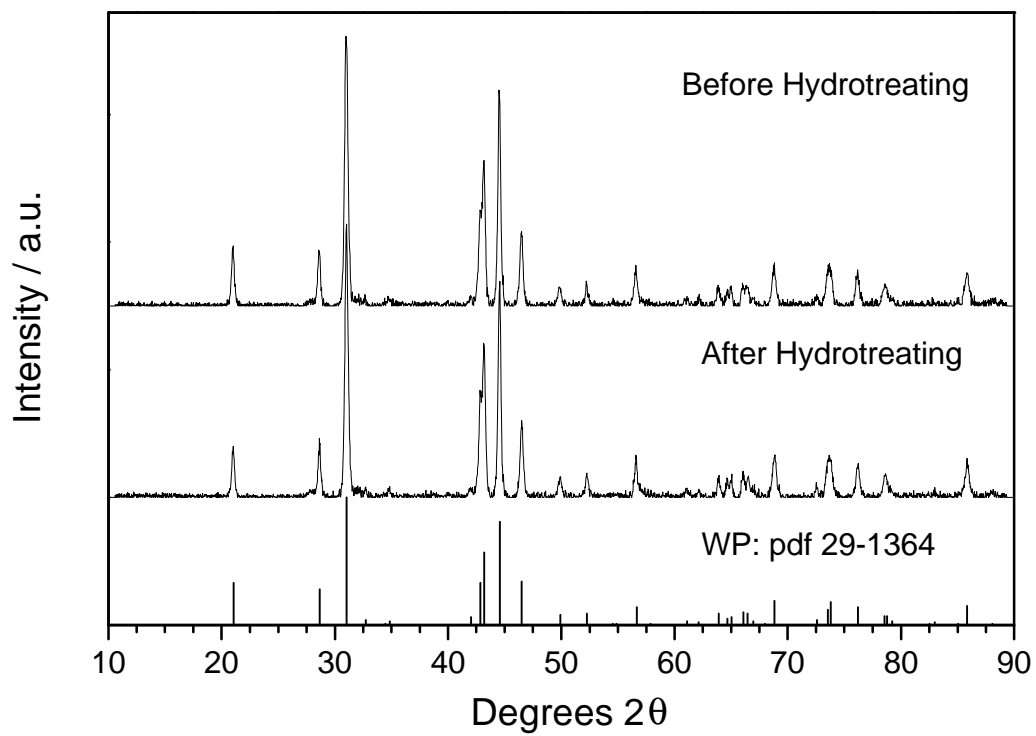| Sample	BET Surface Area m^2 g^{-1}	CO Uptake μmol g^{-1}	Site Density site cm^{-2}
Fresh WP	10	10	6×10^{13}
Spent WP	11	11	6×10^{13}

Figure 2.3: X-ray diffraction patterns of the WP catalyst before and after catalytic reaction.

Table 2.4: Summary of XRD results for tungsten phosphide catalyst before and after reaction.

Lattice Parameter	Fresh WP nm	Spent WP nm	Reference WP[*] nm
a	0.573	0.573	0.573
b	0.325	0.325	0.325
c	0.624	0.623	0.622
Crystallite Size			
$d_{011}(nm)$	246	246	
$S_{011}(m^2g^{-1})$	20	20	

[*]pdf 29-1364

2.3.3. Catalytic Reaction

The tungsten phosphide catalyst was used as a powder, rereduced in the hydroprocessing reactor at 723 K for 2 h. Tungsten sulfide was also used as a powder, but was dispersed in quartz chips, and presulfided at 678 K. Amounts of catalysts corresponding to 30 m^2 were loaded in each catalytic reaction. Quinoline HDN and dibenzothiophene HDS activities of tungsten phosphide are presented in Figure 2.4 as a function of time on stream. The HDN conversion is stable with time, averaging 58% during the last 30 h of reaction. The HDS conversion ranges between 55 and 60% until 30 h, then increases to near 67% for the final 30 h of reaction.
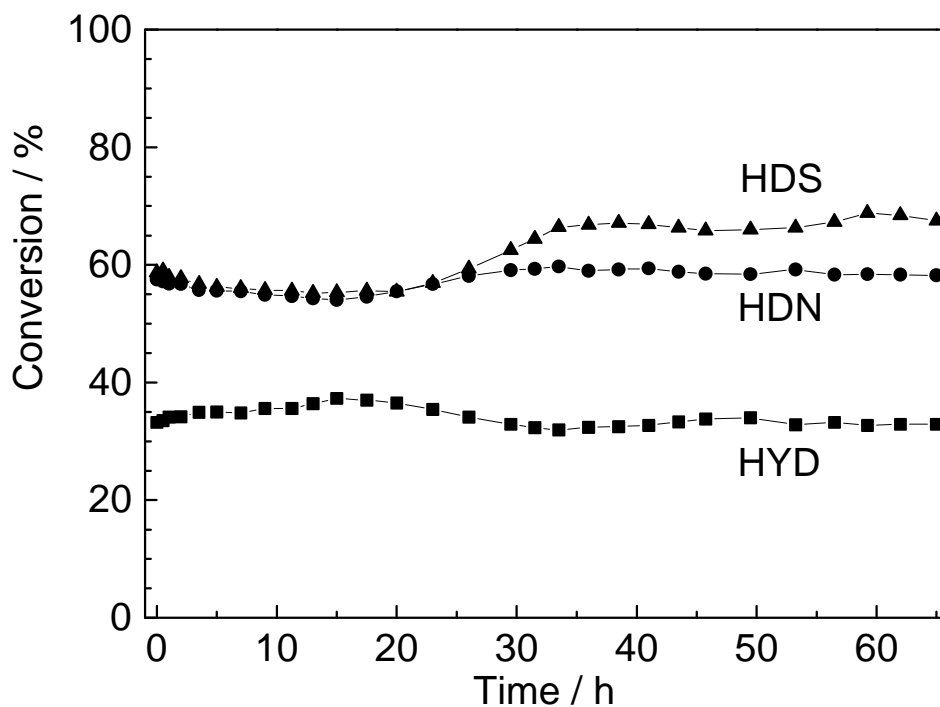
27

Figure 2.4: Hydrotreating performance of tungsten phosphide with time. Definitions: HDS is dibenzothiophene conversion, HDN is the quinoline conversion minus HYD, and HYD is the sum of anilines and tetrahydroquinolines.

Table 2.5 reports the product distributions from hydroprocessing reactions with WP and WS$_2$. The total analysis of the hydroprocessing reaction was complex, as there were over 60 molecules detected in each GC trace; some of which overlapped, were unidentified, or were grouped for simplicity (e.g. there were several isomers of each

alkane). Hence, the information in Table 2.5 is to be considered illustrative. In particular, the results of benzofuran HDO were completely masked by the overlap of decane and benzofuran peaks, and the multiple origins of the products ethylbenzene and/or ethylcyclohexane. Quinoline HDN products are considered to include all of the alkyl C_6 rings, i.e. benzene, cyclohexane, etc… This is prompted by the presence of anilines with cracked alkyl groups, i.e. aniline, methylaniline, and ethylaniline; but does not rule out the possibility of their production from other molecules. Specifically, ethylbenzene and ethylcyclohexane are expected from benzofuran hydrogenation. Cyclohexane is anomalously abundant in the WS_2 run, and probably originated from either dibenzothiophene or tetradecane cracking. The estimates of percents of unsaturated HDN products given in Table 2.5 indicate that saturated HDN products are moderately favored for each catalyst. The product identified from dibenzothiophene HDS were biphenyl and cyclohexylbenzene. The WP catalyst favored unsaturated biphenyl, while the WS_2 yields more of the hydrogenation product cyclohexylbenzene. Tetralin was found to dehydrogenate under our conditions, for which WP was about three times as active as WS_2. The WP had a substantially lower cracking rate for the tetradecane solvent than the WS_2. Hexane was the most abundant alkane cracking product for each catalyst, although it is anomalously abundant in the WP run.

Table 2.5: Product distributions, reported as conversion and selectivity, in

hydroprocessing reactions using WP and WS_2 catalysts.

Quinoline HDN	WP	WS_2
Quinoline Conversion	92	34
Benzene	0.5	2.5
Cyclohexane	1	22
Methylcyclohexane	1	0.5
Toluene	2	3
Ethylcyclohexane	4	2
Ethylbenzene	8	11
Propylcyclohexane	29	1
Propylbenzene	16	1
Aniline	6	0
Methylaniline	2	12
Ethylaniline	1	1
5,6,7,8-Tetrahydroquinoline	13	18
Propylaniline	5	9
1,2,3,4-Tetrahydroquinoline	10	20
Saturated Hydrocarbons	36	25
Unsaturated Hydrocarbons	26	18
Total Hydrocarbons	62	43
PB / (PB + PCH)	35	52
Unsat / (Unsat + Sat)	42	41
Total Anilines	15	21
Total THQs	23	37
Cracked Alkyl Groups	27	54
HDN	58	14

Dibenzothiophene HDS	WP	WS_2
Dibenzothiophene Conversion	67	18
Cyclohexylbenzene	11	67
Biphenyl	89	33

Table 2.5: cont…

Benzofuran HDO	WP	WS$_2$
Benzofuran Conversion	59	45
Ethylbenzene	17	6
Orthoethylphenol	83	94

Tetralin HYD	WP	WS$_2$
Tetralin Conversion	29	11
trans-Decalin	0.7	0.2
cis-Decalin	0.2	0
Naphthalene	99.1	99.8

Tetradecane CRK	WP	WS$_2$
Tetradecane Conversion	2	12
Propane	5	3
Butane	3	7
Pentane	5	12
Hexane	54	15
Heptane	6	12
Octane	5	12
Nonane	6	11
Decane	8	12
Undecane	6	13
Dodecane	3	3

A comparison of hds and hdn conversions of WP to WC, W$_2$N, WS$_2$, and Shell 324 NiMoS/Al$_2$O$_3$ is presented in Figure 2.5. The conversions are directly comparable because the tests were all carried out using equal surface areas loaded in the reactors. As can be seen in Figure 2.4, the amount of uncertainty in the results shown in Figure 2.5 is on the order of 2 percent. The statistical significance of our results may also be estimated by considering results found in Table 3.4, in which five separate catalysts of various loadings were tested based on CO chemisorption values. Those results, whose values
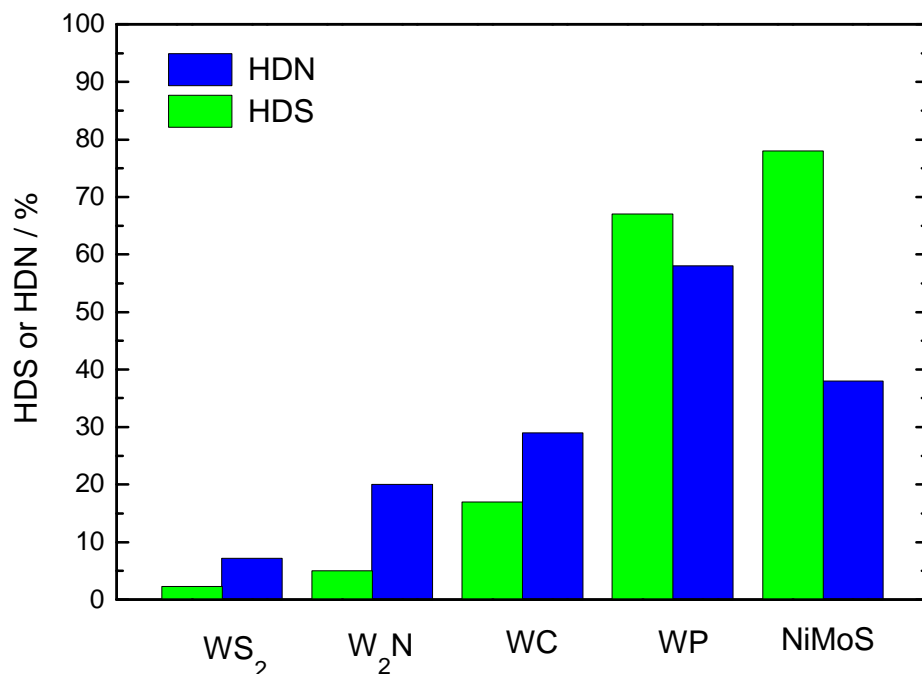
Figure 2.5: Comparison of quinoline HDN and dibenzothiophene HDS conversions of WS$_2$, W$_2$N, WC, WP, and NiMoS/Al$_2$O$_3$ (Shell 324).

include variation based on differences in samples and the use of chemisorption as a basis, have a calculated standard deviation of 4% for HDN and 5% for HDS. The statistical significance of our values is thereby estimated to be about 5% overall. Comparison of the specific rate of hdn reaction on the commercial catalyst can be made with the literature. Specifically, we calculate that the hdn rate on the NiMoS catalyst is 2.1 ± 0.3 e^{-9} mol quinoline s^{-1} m^{-2}, while Satterfield and Yang (44) report results which allow

calculation of a rate of $1.4 \, e^{-9}$ mol quinoline $s^{-1} \, m^{-2}$ on a NiMoS catalyst. Although both

tests employed a three phase catalytic flow reactor, specific differences in the tests

include the pressure (3.1 MPa in our case, 6.9 MPa in the other report), the temperature

(643 K in our case, 648 in the other report), the presence of sulfur (2000 wppm S as

dibenzothiophene in our case, no S in the other report), and the presence of oxygen and

aromatic hydrocarbons in our test, while the other report contains only paraffin solvent.

Although the conditions of the tests were not exactly the same, it is seen that our result is

in reasonable agreement with the previous report.

2.3.4. X-ray Photoelectron Spectroscopy

Fresh and spent WP catalyst samples were characterized by XPS. The fresh sample

was pretreated at 723 K for 2 h in hydrogen flow, then carefully passivated. The spent

WP catalyst was pretreated similarly in helium flow, with the intent to desorb reactant

molecules but not to remove surface sulfide (if present). The atomic concentration

results are reported in Table 2.6. The table reveals that the catalyst sulfides only to a

limited extent, having only 0.8% sulfur in the spent catalyst surface. Also, the

phosphorus content of the surface region decreases slightly following catalytic reaction.

Results of curve fits of the W 4f, W 4d, and P 2p regions are summarized in Table 2.7.

The full width at half maximum of the carbon reference peak is 1.8 eV for both samples,

indicating the absence of deposition of appreciable amounts of carbon deposits or carbide

species during the catalytic reaction.

Table 2.6: XPS atomic percentage results for tungsten phosphide catalyst.

	W	P	O	C	S
Fresh WP	13.2	13.5	53.7	19.5	0.0
Spent WP	13.8	12.0	48.7	24.7	0.8

Table 2.7: XPS curve fit results for tungsten 4f and 4d regions and phosphorus 2p region. Binding energies are reported in eV. Relative amounts are in parentheses.

Sample	W 4f 7/2		W 4d 5/2		P 2p 3/2	
	$W^{\delta+}$	W^{6+}	$W^{\delta+}$	W^{6+}	P^{o}	P^{5+}
Fresh WP	31.8(15)	36.5(37)[†]	243.6(24)	247.9(76)	130.0(18)	134.6(82)
Spent WP	31.9(26)	36.8(41)[†]	244.0(26)	248.0(74)	130.1(24)	134.7(76)

[†] Remainder of W 4f 7/2 region due to interference from O 1s signal

2.4. Discussion

The synthesis of WP by TPR showed the presence of only one transformation feature at close to 900 K (Figure 2.1) and, consistent with this, the XRD analysis of the intermediates (Figure 2.2) show the growth of peaks only due to the phosphide. No features belonging to other species were observed. The final product was a phase pure

tungsten monophosphide, WP (PDF 29-1364), with the MnP type structure (Space Group P$_{bnm}$).

The oxygen to tungsten ratio of the phosphate glass precursor was calculated by the weight change of reduction to be 6.0:1, assuming a stoichiometric WP product. Furthermore, integration of the TPR profile reveals that ~10 % of the water evolution is associated with the water of hydration. These data allow the composition of the amorphous tungsten phosphate starting material to be calculated as $WPO_{5.4} \cdot 0.6H_2O$. This agrees well with the high oxidation states expected for both tungsten and phosphorus, consisting of WO_3 and ½ P_2O_5, i.e. $WPO_{5.5}$, and matches the stoichiometry of $W_2O_3(PO_4)_2$ reported previously for tungsten phosphate (45).

As noted in Figure 2.1, the *in situ* surface area of the sample increased from close to 0.1 m^2 g^{-1} for the starting material to about 11 m^2 g^{-1} for the final WP product. The removal of oxygen from the solid and the coincident increase in density probably accounts for the increase in surface area (46). The surface area probably decreases at higher temperatures by sintering. Estimating the density of the WP phosphate precursor as the average of P_2O_5 (ρ = 2.39 g cm^{-3}) and WO_3 (ρ = 7.16 g cm^{-3}) (47), the density increases from ~4.8 g cm^{-3} for $WPO_{5.5}$ to 8.5 g cm^{-3} for WP. The *in situ* CO uptake also passes through a maximum, tracking the changes in surface area. The *in situ* site density (ratio of CO sites to surface area) increases at high temperature, probably because of removal of residual oxygen from surface sites upon completion of the TPR peak. Still, the *in situ* site density is of the order of 6.0 x 10^{13} atoms cm^{-2}. This value is about an order of magnitude less than the value of 9.6 x 10^{14} atoms cm^{-2} (0.1037 nm^2 per W atom)

calculated from the crystal structure. This indicates that part of the surface may still be blocked by phosphorus or residual oxygen atoms.

The ex situ surface area and CO uptake of the catalysts are reported in Table 2.3. Chemisorption probably occurs on surface vacancies, or coordinatively unsaturated sites, and has been correlated with hydroprocessing performance of materials. Typically, room temperature CO uptake is used for materials with metallic properties such as carbides and nitrides (12, 13), while dry ice temperature O_2 uptake is used for sulfides (48, 49). The O_2 chemisorption in this case is attributed to vacancies at edge sites.

In this study, hydroprocessing of quinoline and dibenzothiophene was carried out at 3.1 MPa and 643 K on 30 m^2 of WP and WS_2, the preparation and properties of which were already described. Previous studies reported the preparation and use of 30 m^2 of WC, W_2N, and $NiMoS/Al_2O_3$ for the same catalytic reaction (13, 31). Briefly, the WC and W_2N were prepared by temperature programmed reduction of WO_3 with methane and ammonia, respectively. The commercial catalyst was presulfided at 678 K for 2 h.

Figure 2.4 shows the time course of reaction for WP. After a period of 30 h in which an equilibrated surface is formed, the catalyst shows constant catalytic activity with no evidence for deactivation. The catalyst is completely stable to the reaction conditions. XRD analysis, shown in Figure 2.3, demonstrates retention of all the lines belonging to WP and the lack of appearance of new peaks after reduction. Similarly, CO chemisorption and BET surface area remained unchanged (Table 2.3) following reaction.

Figure 2.5 summarizes the HDS and HDN conversions of the above mentioned samples.   The tungsten phosphide is observed to be more active than any other tungsten compound for both HDN and HDS, and had a much higher HDN activity than the

commercial NiMoS/Al$_2$O$_3$ catalyst. The catalyst also shows higher activity than MoP

(29), which at the same conditions gives 33% HDN and 13% HDS.

Although the areal comparison of unsupported WP to supported NiMoS may seem to

favor the phosphide, in fact the commercial catalyst is highly optimized and most of its

surface area should be active. Thus, the HDN comparison based on surface area should

give a good approximation of the relative activities of the materials. If, instead of surface

areas, chemisorption quantities (CO for WP, and O$_2$ for NiMoS/Al$_2$O$_3$) are used for

comparison, WP is calculated to be 6.9 times more active than NiMoS/Al$_2$O$_3$. The

calculation is made as follows:

$$\frac{WP}{NiMoS} = \frac{(58\% \ / \ 30 \, m^2)}{(38\% \ / \ 30 \, m^2)} \bullet \frac{(10 \, m^2 \, g^{-1} / \ 10 \, \boldsymbol{m}mol \, g^{-1})}{(160 \, m^2 \, g^{-1} / \ 718 \, \boldsymbol{m}mol \, g^{-1})} = 6.9$$

Stinner *et al.* (30) recently reported that a single MoP site is 6 times more active for HDN

of orthopropylaniline than alumina supported MoS$_2$, based on geometrical estimates of

surface site density. Thus phosphides are promising hydrotreating catalysts.

Table 2.6 reports the atomic concentrations on the surface of the WP catalyst before

and after catalytic reaction. The data indicate the presence of substantial adventitious

carbon and oxygen, as the measurements were carried out on air-exposed catalysts

(though carefully passivated). Nevertheless, the results indicate that the P/W ratio is

close to the stoichiometric value of unity expected for the bulk compound. The

phosphorus content decreases only slightly following the reaction. There is only a small

amount of sulfur on the spent catalyst surface, so the catalyst is tolerant of bulk

sulfidation. The sulfur detected on the spent catalyst amounts to about 3 % of the surface

atoms, counting only W, P, and S. This small amount of sulfur may be helpful for the

HDN process as adsorbed H_2S leads to both acidic (H^+) and basic (S^{2-}) surface sites, which can participate in C-N bond scission (15, 50).

Curve fits of the W 4f, W 4d, and P 2p regions, reported in Table 2.7, reveal that about 75 % of the surface region is oxidized to phosphate and tungstate, and about 25 % is in the reduced phosphide state. Binding energy locations reveal that the oxidation states of W and P in the WP catalyst are near elemental values (39) of 31.4 eV for the W 4f region, 243 eV for the W 4d region, and 130.0 eV for the P 2p region. Chemical shifts near zero have been observed for phosphides of group IV metals previously (51). We report binding energies of the W 4d region because of interference from the O 1s peak in the W 4f region.

It is likely that the oxygen content of the active catalyst is variable, given our experimental conditions. Precedence can be found in the presence of residual oxygen in typical sulfide (4), carbide (13), and nitride (12) catalysts. It was established by TPD experiments that activation at 723K does not remove all of the oxygen from the surface region of WP. Furthermore, it is probable that the depth of the surface oxidation (passivation) layer increases with time, as the phosphide changed color from gray to black (dark blue) with aging after storage for two years. The effects of inclusion of oxygen in the active catalyst surface could be either positive or negative. In previous studies of hydrogenation with Ni_2P (23, 24, 25), a beneficial interaction was identified between surface phosphorus atoms and oxygen. However, a more recent report suggests that aging due to air exposure affected amorphous nickel phosphide and boride catalysts adversely (28). The effect of air exposure on phosphide catalysts may indeed be very

complicated and difficult to reproduce. Our study has been carried out with freshly prepared samples.

Although the surface P/W ratio is close to unity, the phosphorus content of the outermost layer may also be variable. One possibility is that phosphorus covers the surface region of the material similar to the way carbon covers a coked catalyst. In fact, phosphorus deposited on catalyst surfaces via the vapor phase poisoned HDS sites for all transition metals except Ni, where a promotional effect occurred (52). The other extreme in phosphorus distribution is depletion in the outermost layer, possibly by diffusion into the bulk or by vaporization from the surface region. Thus, the catalytic performance of a phosphide sample will likely depend on its preparation history. The extended soak period at 938 K used in the preparation of the WP catalyst may have helped remove trace oxygen impurities, as well as equilibrate the surface region.

Many compounds exist which contain P-S, P-C, and P-N bonds. It is conceivable that phosphorus participates in the catalytic pathway by, for example, creating P-SH sulfhydril sites. Experiments, however, showed no direct interaction between P and H_2S below 973 K (5), although this does not eliminate the possibility of metal catalyzed interactions between heteroatoms. In addition, P/Al_2O_3 reference samples have been found to be inactive in hydroprocessing reactions (53). Thus, the fundamental catalytic benefit of phosphorus in WP is likely to arise from the modification of the nature of tungsten. As mentioned earlier, sulfur on the surface also probably has a positive role in the catalytic reaction chemistry.

XPS results reveal that the oxidation states of both tungsten and phosphorus in WP are near zero. Therefore, the positive effect of alloying is likely to be based on

modification of the electronic structure of the solid. One suggestion, for WC carbide

reforming catalysts, was that the alloying of C and W increases the electron to atom ratio

of tungsten so that its electronic structure resembles platinum (54). Our results do not

contradict the idea that phosphorus could share its electrons with tungsten in such a way

that the electronic structure of tungsten in WP is changed to be similar to noble metals

adjacent on the periodic table, osmium, iridium, and platinum. The sulfides of these

metals are located in the maxima in the 'volcano curves' of activity for both HDN and

HDS reactions (55, 56). The observed trends of HDS and HDN activities in the transition

metal sulfides have also been successfully correlated by a complex combination of

electronic occupation in both d and p orbitals (57).

In commercial phosphorus promoted sulfides, phosphorus is introduced via aqueous

impregnation and interacts strongly with the alumina support, in some cases forming

surface $AlPO_4$ species (5, 58, 59). This leads to changes in the dispersion of the metals,

for example inhibiting formation of nickel or cobalt aluminates, and encourages

crystallization of bulk metal oxides such as MoO_3. Kinetic measurements have revealed

that the presence of phosphorus directly affects the nature of the active sites (60, 61), and

it has been suggested that the role of phosphate is to alter the nature of sites by changing

the stacking of MoS_2 crystallites (62, 63). In contrast to phosphorus promoted sulfide

catalysts, where phosphorus is oxidized and associated with alumina, the phosphorus in

WP is found in reduced form in the bulk.

Tungsten phosphide is highly active for both HDN and HDS reactions in

coprocessing of quinoline and dibenzothiophene. WP resists morphology and phase

changes under hydroprocessing conditions. This conclusion is common to measurements

made by BET surface area, CO chemisorption, X-ray diffraction, and X-ray photoelectron spectroscopy.

2.5.   Conclusions

Tungsten phosphide, WP, was prepared by reduction of an X-ray amorphous phosphate precursor with approximate composition $WPO_{5.5} \cdot 0.5H_2O$. Tungsten phosphide was highly active for hydroprocessing of quinoline and dibenzothiophene in a three phase, fixed bed reactor operated at 643 K and 3.1 MPa. The areal hydrodenitrogenation and hydrodesulfurization rates of WP were both superior to those found for WC, W_2N, and WS_2. The phosphorus in the bulk WP is in a reduced state, which is different from the situation with phosphorus used as a promoter in standard alumina-supported sulfide catalysts. Tungsten phosphide was stable during catalytic testing, showing no signs of bulk sulfiding, sintering, or loss of chemisorption sites. These initial findings demonstrate that WP is one of the most active tungsten compounds yet identified for hydroprocessing reactions.

References

1. Minderhoud, J. K., and van Veen, J. A. R., First-stage hydrocracking: Process and catalytic aspects *Fuel Proc. Tech.* **35**, 87 (1993).
2. Prins, R., Supported metal sulfides *in* "Characterization of Catalytic Materials" (Wachs, I.E. and Fitzpatrick, L.E. Eds.), p. 109. Butterworth-Heinemann, Boston, MA, 1992.
3. Grange, P., Catalytic hydrodesulfurization *Cat. Rev. Sci. Eng.* **21**(1), 135 (1980).
4. Furimski, E., Role of MoS_2 and WS_2 in hydrodesulfurization *Cat. Rev. Sci. Eng.* **22**(3), 371 (1980).
5. Iwamoto, R., and Grimblot, J., Influence of phosphorus on the properties of alumina-based hydrotreating catalysts *Adv. Cat.* **44**, 417 (1999).
6. Cruz Reyes, J., Avalos-Borja, M., Lopez Cordero, R., and Lopez Agudo, A., Influence of phosphorus on the structure and the hydrodesulfurization and hydrodenitrogenation activity of W/Al_2O_3 catalysts *Appl. Cat. A* **120**, 147 (1994).
7. Atanasova, P., Tabakova, T., Vladov, Ch., Halachev, T., and Lopez Agudo, A., Effect of phosphorus concentration and method of preparation on the structure of the oxide form of phosphorus-nickel-tungsten/alumina hydrotreating catalysts *Appl. Cat. A* **161**, 105 (1997).
8. Atanasova, P., and Lopez Agudo, A., Infrared studies of nitric oxide adsorption on reduced and sulfided P-Ni-Mo/Al_2O_3 catalysts *Appl. Cat. B* **5**(4), 329 (1995).
9. Poulet, O., Hubaut, R., Kasztelan, S., and Grimblot, J., Experimental evidences of the direct influence of phosphorus on activity and selectivity of a MoS_2-γAl_2O_3 hydrotreating catalyst *Bull. Soc. Chim. Belg.* **100**(11-12), 857 (1991).
10. Callant, M., Holder, K. A., Grange, P., and Delmon, B., Effect of H_2S and H_2 partial pressures on the hydrodenitrogenation (HDN) of aniline and indole over a NiMoP-γAl_2O_3 catalyst *Bull. Soc. Chim. Belg.* **104**(4-5), 245 (1995).
11. Oyama, S. T., Yu, C. C., and Ramanathan, S., Transition metal bimetallic oxycarbides: synthesis, characterization, and activity studies *J. Catal.* **184**, 535 (1999).
12. Ramanathan, S., Yu, C. C., and Oyama, S. T., New catalysts for hydroprocessing: bimetallic oxynitrides *J. Catal.* **173**, 1 (1998).
13. Ramanathan, S., and Oyama, S. T., New catalysts for hydroprocessing: transition metal carbides and nitrides *J. Phys. Chem.* **99**, 16365 (1995).
14. Danot, M., Afonso, J., Portefaix, J. L., Breysse, M., and des Couries, T., Catalytic properties of niobium sulfides in the conversion of nitrogen containing molecules *Catal. Today* **10**, 629 (1991).
15. Cattenot, M., Portefaix, J.-L., Afonso, J., Breysse, M., Lacroix, M., and Perot, G., Mechanism of carbon-nitrogen bond scission on unsupported transition metal sulfides *J. Catal.* **173**, 366 (1998).
16. Janssens, J.-P., Dick van Langeveld, A., Moulijn, J. A., Characterization of alumina- and silica-supported vanadium sulfide catalysts and their performance in hydrotreating reactions *Appl. Catal. A* **179**(1-2), 229 (1999).
17. Quartararo, J., Mignard, S., and Kasztelan, S., Hydrodesulfurization and hydrogenation activities of alumina-supported transition metal sulfides *J. Catal.* **192**, 307 (2000).
18. Joo, H. S., and Guin, J. A., Activity of nobel metal-promoted hydroprocessing catalysts for pyridine HDN and naphthalene hydrogenation *Fuel. Proc. Tech.* **49**, 137 (1996).
19. Qian, W., Yoda, Y., Hirai, Y., Ishihara, A., and Kabe, T., Hydrodesulfurization of dibenzothiophene and hydrogenation of phenanthrene on alumina-supported Pt and Pd catalysts *Appl. Catal. A* **184**, 81 (1999).
20. Cowan, R., H☐lin, M., Reinink, H., Jesbaert, J., and Chadwick, D., Influence of ammonia on thiophene HDS at high pressures over nobel metal catalysts for deep HDS applications *Catal. Today* **45**, 381 (1998).
21. Song, C., and Reddy, K. M., Mesoporous molecular sieve MCM-41 supported Co-Mo catalysts for desulfurization of dibenztothiophene in distillate fuels *Appl. Catal. A* **176**, 1 (1999).
22. Song, C., Designing sulfur-resistant, nobel-metal hydrotreating catalysts *Chemtech* **29**, 26 (1999).
23. Nozaki, F., and Adachi, R., Chemical composition of the catalysts prepared by reduction of nickel orthophosphate in hydrogen and catalytic activity for partial hydrogenation of 1,3-butadiene *J. Catal.* **40**, 166 (1975).

24. Nozaki, F., Kitoh, T., Sodesawa, T., Promoting effect of oxygen for hydrogenation of butadiene over Ni_2P catalysts *J. Catal.* **62**, 286 (1980).

25. Nozaki, F., and Tokumi, M., Hydrogenation activity of metal phosphides and promoting effect of oxygen *J. Catal.* **79**, 207 (1983).

26. Muetterties, E. L., and Sauer, J. C., Catalytic properties of metal phosphides. I. Qualitative assay of catalytic properties *J. Am. Chem. Soc.* **96**(11), 3410 (1974).

27. van Veen, J. A. R., and de Beer, V. H. J., Phosphorus promotion of Ni(Co)-containing Mo-free catalysts in quinoline hydrodenitrogenation *J. Catal.* **161**, 539 (1996).

28. Lee, S.-P., Chen, Y.-W., Nitrobenzene hydrogenation on Ni-P, Ni-B, and Ni-P-B ultrafine materials *J. Mol. Catal. A* **152**, 213 (2000).

29. Li, W., Dhandapani, B., and Oyama, S. T., Molybdenum Phosphide: A novel catalyst for hydrodenitrogenation *Chem. Lett.* 207 (1998).

30. Stinner, C., Prins, R., and Weber, Th., Formation, structure, and HDN activity of unsupported molybdenum phosphide *J. Catal.* **191**, 438 (2000).

31. Lucy, T., St. Clair, T., and Oyama, S. T.*,* Synthesis, characterization, and reactivity of tungsten oxynitride *J. Mater. Res.* **13**, 2321 (1998).

32. Shi, L., Wang, X. P., and Xin, Q., Catalytic activity and selectivity of supported W_2N hydrodenitrogenation catalyst *Chin. Chem. Lett.* **6**(9), 819 (1995).

33. Frety, R., Breysse, M., Lacroix, M., and Vrinat, M., Unsupported MoS_2 and WS_2 model catalysts: Influence of textural properties on hydrodesulfurization and hydrodenitrogenation activities *Bull. Soc. Chim. Belg.* **93**(8-9), 663 (1984).

34. Vrinat, M., Lacroix, M., Breysse, M., and Frety, R., A Comparison of some catalytic properties of unsupported MoS_2 and WS_2 catalyts promoted by group VIII metals *Bull. Soc. Chim. Belg.* **93**(8-9), 697 (1984).

35. Ramanathan, K., and Weller, S. W., Characterization of tungsten sulfide catalysts *J. Catal.* **95**, 249 (1985).

36. Alonso, G., Del Valle, M., Cruz, J., Licea-Claverie, A., Petranovskii, V., and Fuentes, S., Preparation of MoS_2 and WS_2 catalysts by *in situ* decomposition of ammonium thiosalts *Catal. Lett.* **52**, 55 (1998).

37. Cullity, B. D. "Elements of X-ray Diffraction," 2nd ed., p. 102. Addison-Wesley, Menlo Park, CA, 1978.

38. Falconer, J. L., and Schwartz, K. A., *Cat. Rev. Sci. Eng.* **25**, 141 (1983).

39. "Handbook of X-ray Photoelectron Spectroscopy" (J.F. Moulder; W.F. Stickle; P.E. Sobol; K.D. Bomben; and J. Chastain, Eds) Perkin Elmer Company, Eden Prairie, MN, 1992.

40. Aronsson, B., Lundstrom, T., and Rundqvist, S. "Borides, Silicides, and Phosphides," p. 65, John Wiley and Sons, New York, NY, 1965.

41. Rundqvist, S., *Acta Chem. Scand.* Phosphides of the B31 (MnP) structure type **16**(2), 287 (1962).

42. Tremel, W., Hoffmann, R., and Silvestre, J., Transition between NiAs and MnP type phases: an electronically driven distortion of triangular (3^6) nets *J. Am. Chem. Soc.* **108**, 5174 (1986).

43. Schönberg, N., An x-ray investigation of transition metal phosphides *Acta Chem. Scand.* **8,** 226 (1954).

44. Satterfield, C. N., and Yang, S. H., Catalytic hydrogenation of quinoline in a trickle-bed reactor. Comparison with vapor phase reaction *Ind. Eng. Chem. Process Des. Dev.* **23**, 11 (1984).

45. Gopalakrishnan, J., Pandey, S., and Rangan, K. K., Convenient route for the synthesis of transition-metal pnictides by direct reduction of phosphate, arsenate, and antimonate precursors *Chem Mater.* **9**, 2113 (1997).

46. Fenelonov, V. B., The porous structure of products of topochemical reactions *Kin. and Catal.* **35**(5), 736 (1994).

47. "CRC Handbook of Chemistry and Physics" 66th edition, Weast, R. C., Astle, M. J., and Beyer, W. H., Eds. CRC Press, Boca Raton, FL (1986).

48. Zmeirczak, W., Muralidhar, G., and Massoth, F. E., *J. Catal* **77**, 432 (1982).

49. Bodrero, T. A., and Batholomew, C. H., *J. Catal.* **78**, 253 (1982).

50. Yang, S. H., and Satterfield, C. N., Some effects of sulfiding of a $NiMo/Al_2O_3$ catalyst on its activity for hydrodenitrogenation of quinoline *J. Catal.* **81**, 168 (1983).

51. Myers, C. E., Franzen, H. F., and Anderegg, J. W., X-ray photoelectron spectra and bonding in transition-metal phosphides *Inorg. Chem.* **24**(12), 1822 (1985).

52. Eijsbouts, S., van Gestel, J. N. M., van Oers, E. M., Prins, R., van Veen, J. A. R., and de Beer, V. H. J., In situ poisoning of the thiophene hydrodesulfurization activity of carbon-supported transition metal sulfide catalysts *Appl. Catal. A* **119**, 292 (1994).

53. Jian, M., and Prins, R., The effect of phosphorus on the HDN reaction of piperidine, decahydroquinoline, and ortho-propylaniline over Ni-MoS$_2$/Al$_2$O$_3$ catalysts *Catal. Lett.* **35**, 193 (1995).

54. Levy, R.B., and Boudart, M., Platinum-like behavior of tungsten carbide in surface catalysis *Science* **181**, 457 (1973).

55. Eijsbouts, S., de Beer, V. H. J., and Prins, R., Hydrodenitrogenation of quinoline over carbon-supported transition metal sulfide catalysts *J. Catal.* **127**, 619 (1991).

56. Pecoraro, T. A., and Chianelli, R. R., Hydrodesulfurization catalysis by transition metal sulfides *J. Catal.* **67**, 430 (1981).

57. Harris, S., and Chianelli, R. R., Catalysis by transition metal sulfides: The relation between calculated electronic trends and HDS activity *J. Catal.* **86**, 400 (1984).

58. Morales, A., Ramirez de Agudelo, M. M., and Hernandez, F., Adsorption mechanism of phosphorus on alumina *Appl. Catal.* **41**, 261 (1988).

59. Gishti, K., Iannibello, A., Marengo, S., Morelli, G., and Tittarelli, P., On the role of phosphate anion in the MoO$_3$-Al$_2$O$_3$ based catalysts *Appl. Catal.* **12**, 381 (1984).

60. Jian, M., and Prins, R., Existence of different catalytic sites in HDN catalysts *Catal. Today* **30**, 127 (1996).

61. Jian, M., and Prins, R., Mechanism of the hydrodenitrogenation of quinoline over NiMo(P)/Al$_2$O$_3$ catalysts *J. Catal.* **179**, 18 (1998).

62. Prins, R., Jian, M., Flechsenhar, M., Mechanism and kinetics of hydrodenitrogenation *Polyhedron* **16**(18), 3235 (1997).

63. Ryan, R. C., Kemp, R. A., Smegal, J. A., Denley, D. R., and Spinnler, G. E., Stacking of molybdenum disulfide layers in hydrotreating catalysts *Stud. Surf. Sci. Catal.* **50**, 21 (1989).